

# Linear stability of flow in an internally heated rectangular duct

By MARKUS UHLMANN<sup>1</sup> AND MASATO NAGATA<sup>2</sup>

<sup>1</sup>Departamento de Combustibles Fósiles, CIEMAT, 28040 Madrid, Spain

<sup>2</sup>Department of Aeronautics and Astronautics, Graduate School of Engineering,  
Kyoto University, Kyoto 606-8501, Japan

(Received 20 April 2005 and in revised form 13 September 2005)

The linear stability of flow in a vertical rectangular duct subject to homogeneous internal heating, constant-temperature no-slip walls and a driving pressure gradient is investigated numerically in the framework of the Boussinesq hypothesis. A Galerkin method based upon modified Chebyshev polynomials is used to discretize the linearized Navier–Stokes equations in their most compact form, i.e. eliminating the pressure and the streamwise velocity and making use of the intrinsic symmetry properties. A classification of the basic flow in Grashof and Reynolds space in terms of inflectional properties is proposed. It is found that the flow loses stability at all aspect ratios for a combination of finite thermal buoyancy and pressure forces with opposed signs. In the square duct, the unstable region lies inside the range where the basic velocity profile exhibits additional inflection lines. Unstable eigenfunctions are obtained for all basic symmetry modes, consisting of rapidly propagating large-scale structures located in the vicinity of the inflection lines near the centre of the duct.

---

## 1. Introduction

Pressure-driven flow through a straight duct with a rectangular cross-section occurs in a wide range of technical applications. A large number of past studies of this flow have focused upon the origin of secondary motion which is observed in the corner region for turbulent conditions (e.g. Gavrilakis 1992; Galletti & Bottaro 2004). By contrast, the transition process from the laminar state to turbulence in this configuration has received less attention. A notable exception is the numerical study of Tatsumi & Yoshimura (1990) who established that the laminar flow in a rectangular duct is stable with respect to all infinitesimal perturbations below a critical aspect ratio of 3.2, where the aspect ratio is defined in the range from unity to infinity. Theofilis, Duck & Owen (2004) later confirmed the stabilizing effect of the sidewalls through linear analysis performed at higher spatial resolution. The linear theory is thus incapable of predicting the flow instability in the rectangular duct with a small aspect ratio. Moreover, for cross-sections with an aspect ratio above the critical value it yields a gross over-prediction of the critical Reynolds number when compared to the experimentally measured values of Kao & Park (1970). On the other hand, no attempts to identify fully nonlinear (steady or travelling-wave) solutions for finite geometrical aspect ratios have been reported in the literature.

Nonlinear studies usually rely upon a continuation technique which, starting from a suitable initial guess, allows us to track a solution in parameter space. One such

example can be found in the work of Ehrenstein & Koch (1991) who were able to find wave-like solutions in plane Poiseuille flow (PPF) at Reynolds numbers as low as experimentally determined transition values.

Since the flow in the low-aspect-ratio rectangular duct (and, particularly, the square duct) is linearly stable, there exists no obvious initial condition for starting a continuation procedure. In analogous situations, the method of homotopy has proved to be a valuable tool: by embedding the problem into a related one with desirable linear instability characteristics, both being smoothly connected by a single parameter, nonlinear solutions can often be obtained for the original problem. This technique has been successfully employed by Nagata (1990) in plane Couette flow, by Waleffe (2001) in PPF and by Wedin & Kerswell (2004) in pipe flow.

The object of the present study is twofold. First, we intend to provide a basis for a subsequent nonlinear analysis of the flow in a rectangular duct with small aspect ratio. For this purpose, we have chosen to perform a linear stability analysis of the duct flow including a homogeneously distributed heat source. This choice of the homotopy parameter is motivated by the work of Nagata & Generalis (2002) and Generalis & Nagata (2003) on internally heated PPF (HPPF) where the basic velocity profile has inflection points in a certain parameter range, leading to the appearance of a family of new linear modes with positive growth rates. By analogy, adding a heat source to the otherwise linearly stable flow in a rectangular duct has the prospect of yielding unstable perturbations which in turn will permit a continuation procedure to be applied in the future. As it turns out in the present case, the temperature fluctuations must be taken into account (i.e. the Prandtl number must be finite) in order to lead to linear instability of the flow in the square duct.

Our second object is to elucidate the linear stability characteristics of the flow with an internal heat source in its own right. This problem deserves attention because of a number of important applications: the heat release created by an electric current in a conducting fluid (Kikuchi, Shioyama & Kawara 1986), radiative heating of fluids owing to microwaves (Gilchrist, Kriegsmann & Papageorgiou 1998), solar radiation in planetary atmospheres (Tritton 1975), chemically reacting fluid mixtures and internal heating owing to nuclear reactions (Nourgaliev & Dinh 1997). Radioactive internal heating further plays a role in the study of the motion of the Earth's mantle (Roberts 1967; Tritton & Zarraga 1967; McKenzie, Roberts & Weiss 1974). To our knowledge, the problem of stability of the flow in an internally heated rectangular duct has not previously been considered in the literature, probably owing to the large parameter space and system size which require substantial computational resources.

The organization of this paper is as follows. We first establish the mathematical formulation of the linear stability problem and then describe our numerical method. In section §4, we present a classification of the basic flow in terms of its inflectional properties. We then briefly revisit the isothermal case in the rectangular duct and present additional data on the HPPF case before we turn to the main results of our analysis. The paper closes with a short discussion in §5.

## 2. Mathematical formulation

We consider the flow in a straight duct with rectangular cross-section. The Cartesian coordinates are  $(x, y, z)$  with  $x$  being the axial direction and the corresponding unit vectors are  $\hat{x}$ ,  $\hat{y}$ ,  $\hat{z}$ . The flow domain is  $\Omega = \mathbb{R} \times [-b, b] \times [-c, c]$ . The aspect ratio is defined as  $A = c/b \geq 1$ , with the limit  $A \rightarrow \infty$  corresponding to flow in a plane channel. Gravity acts in the negative axial direction, i.e.  $\mathbf{g} = -g\hat{x}$ . The fluid with

density  $\rho$ , viscosity  $\nu$  and thermal conductivity  $\kappa$  is subjected to a homogeneously distributed internal heat source with intensity  $q$ . We adopt the Boussinesq hypothesis with a coefficient of thermal expansion  $\alpha_T$ . Using  $b$ ,  $b^2/\nu$ ,  $\nu/b$ ,  $\rho\nu^2/b^2$ ,  $\nu^2/(g\alpha_T b^3)$  as reference values for length, time, velocity, pressure and temperature, the flow equations take the following form:

$$\partial_t \mathbf{u} + (\mathbf{u} \cdot \nabla) \mathbf{u} = -\nabla p + T \hat{\mathbf{x}} + \nabla^2 \mathbf{u}, \tag{2.1a}$$

$$\nabla \cdot \mathbf{u} = 0, \tag{2.1b}$$

$$\partial_t T + (\mathbf{u} \cdot \nabla) T = \frac{1}{Pr} \nabla^2 T + \frac{2Gr}{Pr}, \tag{2.1c}$$

where  $\mathbf{u}$  is the velocity vector,  $p$  the pressure,  $T$  the temperature,  $Pr = \nu/\kappa$  the Prandtl number and  $Gr = g\alpha_T q b^5 / (2\nu^2 \kappa)$  the Grashof number. The duct is bounded by no-slip walls ( $\mathbf{u} = 0$ ) which are kept at a constant temperature ( $T = 0$ ). The basic flow is assumed uni-directional and independent of the streamwise coordinate, i.e. the basic velocity  $\mathbf{U} = U(y, z) \hat{\mathbf{x}}$  and the basic temperature distribution  $\Theta(y, z)$  obey the following equations:

$$(\partial_{yy} + \partial_{zz})U = -\Theta - \chi Re, \tag{2.2a}$$

$$(\partial_{yy} + \partial_{zz})\Theta = -2Gr. \tag{2.2b}$$

The axial pressure-gradient term  $\chi Re$  in equation (2.2a) is obtained from the equivalent pressure-driven isothermal case. The parameter  $\chi$  is chosen such that  $(\partial_{yy} + \partial_{zz})U_{iso} = -\chi$  leads to  $U_{max,iso} = \max(U_{iso}) = 1$  and the Reynolds number is defined as  $Re = U_{max,iso} b/\nu$ . Thereby,  $\chi$  is a function of the aspect ratio  $A$  alone and the Reynolds number controls the amplitude of the pressure-gradient. Note that the Reynolds number can take positive or negative values, according to the sign of the driving pressure-gradient.

The perturbation component of the field is expanded in normal modes with real axial wavenumber  $\alpha$  and complex frequency  $-\alpha c$ :

$$[\mathbf{u}'(\mathbf{x}, t), p'(\mathbf{x}, t), \theta'(\mathbf{x}, t)] = [\mathbf{u}(y, z), p(y, z), \theta(y, z)] e^{i\alpha(x-ct)}. \tag{2.3}$$

Elimination of the axial velocity component and the pressure leads to the following linear perturbation equations for the velocity components  $v$ ,  $w$  and the temperature  $\theta$ :

$$\mathcal{E}_{yz} v - \partial_y \theta = \mathcal{O}_{yz} w, \tag{2.4a}$$

$$\mathcal{E}_{zy} w - \partial_z \theta = \mathcal{O}_{zy} v, \tag{2.4b}$$

$$(ci\alpha Pr + i\alpha U Pr + \alpha^2 - \partial_{yy} - \partial_{zz})\theta + Pr(\partial_y \Theta)v + Pr(\partial_z \Theta)w = 0, \tag{2.4c}$$

where  $\mathcal{E}$ ,  $\mathcal{O}$  are equivalent to the even and odd operators defined in Tatsumi & Yoshimura (1990) except for the choice of the reference values:

$$\mathcal{E}_{\beta\gamma} = -\left[ \frac{i}{\alpha} (\partial_{\beta\beta} + \partial_{\gamma\gamma} - \alpha^2) + (U - c) \right] (\partial_{\beta\beta} - \alpha^2) + (\partial_{\beta\beta} U), \tag{2.5a}$$

$$\mathcal{O}_{\beta\gamma} = \left[ \frac{i}{\alpha} (\partial_{\beta\beta} + \partial_{\gamma\gamma} - \alpha^2) + (U - c) \right] \partial_{\beta\gamma} - (\partial_\gamma U) \partial_\beta + (\partial_\beta U) \partial_\gamma - (\partial_{\beta\gamma} U). \tag{2.5b}$$

The appropriate boundary conditions for the perturbations are the following:

$$y = \pm 1 : v = w = \partial_y v = \theta = 0, \quad z = \pm A : v = w = \partial_z w = \theta = 0. \tag{2.6}$$

	Homogeneous Dirichlet	Homogeneous Dirichlet and homogeneous Neumann
	$\phi_j^D(x) \quad \forall \quad j = 1, 2, 3, \dots$	$\phi_j^N(x) \quad \forall \quad j = 2, 3, \dots$
Even	$T_{2j}(x) - T_0(x)$	$T_{2j}(x) + (j^2 - 1)T_0(x) - j^2T_2(x)$
Odd	$T_{2j+1}(x) - T_1(x)$	$T_{2j+1}(x) + \frac{j^2+j-2}{2}T_1(x) - \frac{j^2+j}{2}T_3(x)$

TABLE 1. One-dimensional basis functions  $\phi_j(x)$  based upon Chebyshev polynomials  $T_k(x)$  for even/odd parity and different end-point conditions.

In the limit of vanishing Grashof number, the pure pressure-driven case of Tatsumi & Yoshimura (1990) is recovered; for vanishing Prandtl number, the stability problem becomes purely hydrodynamical, albeit for a modified basic flow.

Examination of equations (2.4) and taking into account that the basic flow is an even function of both  $y$  and  $z$  shows that the perturbations are restricted to the same four basic symmetry modes (hereinafter modes I–IV) as found in Tatsumi & Yoshimura (1990). The temperature perturbations  $\theta$  follow the same symmetry as the axial velocity, namely,

$$\left. \begin{aligned} \text{I: } & u(o,e) \quad v(e,e) \quad w(o,o) \quad p(o,e) \quad \theta(o,e), \\ \text{II: } & u(o,o) \quad v(e,o) \quad w(o,e) \quad p(o,o) \quad \theta(o,o), \\ \text{III: } & u(e,e) \quad v(o,e) \quad w(e,o) \quad p(e,e) \quad \theta(e,e), \\ \text{IV: } & u(e,o) \quad v(o,o) \quad w(e,e) \quad p(e,o) \quad \theta(e,o). \end{aligned} \right\} \quad (2.7)$$

The notation of (2.7) is such that e.g. (o,e) stands for an odd parity in  $y$  and an even parity in  $z$ . Note that modes I and IV are equivalent in the case of a square domain  $A = 1$ .

### 3. Numerical method

The basic flow equations (2.2) were solved with the fast Chebyshev–Galerkin method of Shen (1995), using  $256 \times 256$  modes. Excellent agreement with tabulated values of Tatsumi & Yoshimura (1990) in the limit of vanishing Grashof number was obtained.

The perturbation functions in the cross-stream plane are expanded as follows:

$$v(y, z) = \sum_{m=2}^{N_y} \sum_{n=1}^{N_z} \hat{v}_{mn} \phi_m^N(y) \phi_n^D(z), \quad (3.1a)$$

$$w(y, z) = \sum_{m=1}^{N_y} \sum_{n=2}^{N_z} \hat{w}_{mn} \phi_m^D(y) \phi_n^N(z), \quad (3.1b)$$

$$\theta(y, z) = \sum_{m=1}^{N_y} \sum_{n=1}^{N_z} \hat{\theta}_{mn} \phi_m^D(y) \phi_n^D(z), \quad (3.1c)$$

where the one-dimensional basis functions are the modified Chebyshev polynomials given in table 1. The system (3.1) automatically satisfies the boundary conditions, which eliminates spurious eigenvalues. By using basis functions with combinations of odd/even parity corresponding to the present basic symmetry modes, a further reduction of the system dimension is achieved. When comparing the present results

$N_y \times N_z$	$\text{Re}(c)/Re$	$\text{Im}(c)/Re$
$10 \times 20$	0.559622	$0.22787675 \times 10^{-1}$
$15 \times 30$	0.232026	$0.10520835 \times 10^{-3}$
$20 \times 30$	0.232165	$0.13115827 \times 10^{-3}$
$20 \times 35$	0.232342	$-0.12105729 \times 10^{-4}$
$25 \times 40$	0.232386	$-0.24038751 \times 10^{-4}$
$30 \times 45$	0.232392	$-0.22714486 \times 10^{-4}$
$35 \times 50$	0.232392	$-0.22017663 \times 10^{-4}$
$40 \times 60$	0.232392	$-0.21974008 \times 10^{-4}$

TABLE 2. Convergence of the least stable mode (symmetry I) for iso-thermal flow in a rectangular duct of aspect ratio  $A = 5$  at Tatsumi & Yoshimura's critical point ( $Re = 10\,400$  and  $\alpha = 0.91$ ). Note that the phase velocity is normalized with the Reynolds number for consistency with the choice of reference values used by Tatsumi & Yoshimura (1990).

to other studies, it should be kept in mind that a truncation level  $N_y$  corresponds to Chebyshev polynomials up to degree  $2N_y$  ( $2N_y + 1$  in the odd case).

We have examined a collocation method (using Gauss–Lobatto collocation points on the half-interval) and a full Galerkin method. It was found that while both methods consistently reproduce the relevant eigenvalues, the collocation method yields additional spurious modes. The drawback of the Galerkin method is a higher complexity of the code and longer execution times for the matrix assembly. However, we prefer the Galerkin approach because of its reliability. The final generalized eigenvalue problem was solved by means of the QZ algorithm and using 64 bit arithmetic. For a truncation level of  $N_y = N_z = 20$  ( $N_y = N_z = 30$ ), the memory requirement of the present code is 54 MB (240 MB) and the execution time 147 s (2978 s) on an Intel Pentium IV processor with a clock frequency of 3 GHz.

The present method was thoroughly tested. Excellent agreement with the results of Tatsumi & Yoshimura (1990) and Theofilis *et al.* (2004) in the limit of vanishing Grashof and Prandtl numbers was obtained. Table 2 shows the numerical convergence of the least stable mode for the duct with aspect ratio  $A = 5$  at Tatsumi & Yoshimura's critical point ( $Re = 10\,400$  and  $\alpha = 0.91$ ). Furthermore, the results of Nagata & Generalis (2002) and Generalis & Nagata (2003) in a plane channel for finite Grashof number and different values for the Prandtl number were recovered in the limit of large aspect ratio. Additional details of the numerics and the validation procedure can be found in Uhlmann (2004).

## 4. Results

### 4.1. Inflectional properties of the basic flow

An important characteristic of the basic velocity profile with relevance to stability analysis is the existence of inflection points. For the present two-dimensional case, we use the definition of Kawahara *et al.* (1998) and call inflection points those locations in the cross-stream plane where the second derivative of the basic velocity in the direction of its gradient is zero,  $d^2U/d\mathbf{n}^2 = 0$ , with the unit vector defined as  $\mathbf{n} = \nabla U / |\nabla U|$ . It turns out that in the square duct there are five different types of basic flow, which will be called  $M_1$  to  $M_5$  in the following. Their occurrence in the  $(Re, Gr)$ -plane is depicted in figure 1(a) (only the upper half-plane is shown since the other half-plane is recovered by symmetry with respect to the origin) and examples

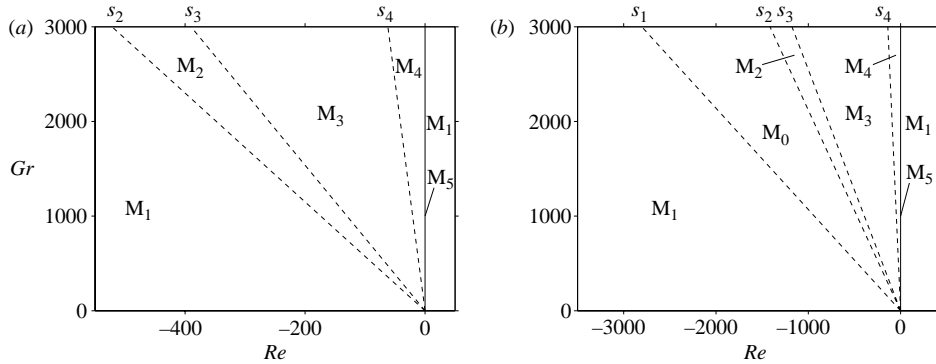


FIGURE 1. The regions in the upper half of the  $(Re, Gr)$ -plane where the observed basic flow types  $M_i$  occur. Note that  $M_1$  includes the  $Gr=0$  axis;  $M_5$  corresponds exclusively to the  $Re=0$  axis. Region  $M_0$  is only defined for finite aspect ratios larger than unity. The slopes  $s_i$  of the dividing lines defined by  $Gr = s_i Re$  are given in table 3 for various aspect ratios. (a)  $A = 1$ ; (b)  $A = 3$ .

for each region are plotted in figure 2. In region  $M_1$ , which includes the  $Gr = 0$  axis, the basic flow has a shape similar to pure pressure-driven flow, i.e. there are 4 closed inflection lines, one attached to each corner. When crossing from zone  $M_1$  into zone  $M_2$ , 9 new inflection lines appear simultaneously, one circular-shaped line located in the center of the channel and 2 smaller elongated closed lines in each quadrant. Upon entering region  $M_3$ , the inflectional pattern remains similar to  $M_2$ , but both positive and negative basic flow occurs (reverse flow). When approaching the border between  $M_3$  and  $M_4$ , the central inflection line deforms and increases its circumference while the 8 smaller elongated lines move towards the corners of the domain. These latter lines as well as the 4 lines attached to the corners shrink until they disappear at the border with region  $M_4$ . The flow has fully reversed its direction in zone  $M_4$  and the inflectional pattern has turned into a single inflectional line. Finally, figure 2 shows that the flow on the  $Re = 0$  axis  $M_5$  is characterized by a single open inflection line close to each corner. In the quadrants where the Reynolds and Grashof numbers have the same sign, the basic flow exhibits the same shape as in zone  $M_1$ .

In configurations with an aspect ratio larger than unity, the above characterization of the basic flow still applies, although the exact shape of the inflection lines obviously changes. The diagram in the  $(Re, Gr)$ -plane valid for  $A > 1$  is shown in figure 1 (b). When starting in zone  $M_1$  (quadrant II) and continuously increasing the Reynolds number, two inflection lines which do not cross the minor axis ( $z = 0$ ) appear first near the origin. The corresponding basic flow type – which has no counterpart in the square case – will be called  $M_0$ . With a further increase in the Reynolds number, those two inflection lines join into a single one which crosses both coordinate axes. This conversion determines the boundary between zones  $M_0$  and  $M_2$ . The definition of the remaining regions is strictly the same as in the square case. Why is the distinction between  $M_0$  and  $M_2$  important? In the limit of infinite aspect ratio, the basic flow velocity depends solely on the  $y$ -coordinate (Nagata & Generalis 2002),

$$U = \frac{1}{12} Gr(y^4 - 6y^2 + 5) + Re(1 - y^2), \quad (4.1)$$

with inflection curves being lines of constant  $z$ . Even for large but finite aspect ratios it is expected that the basic flow properties in the direction of the minor

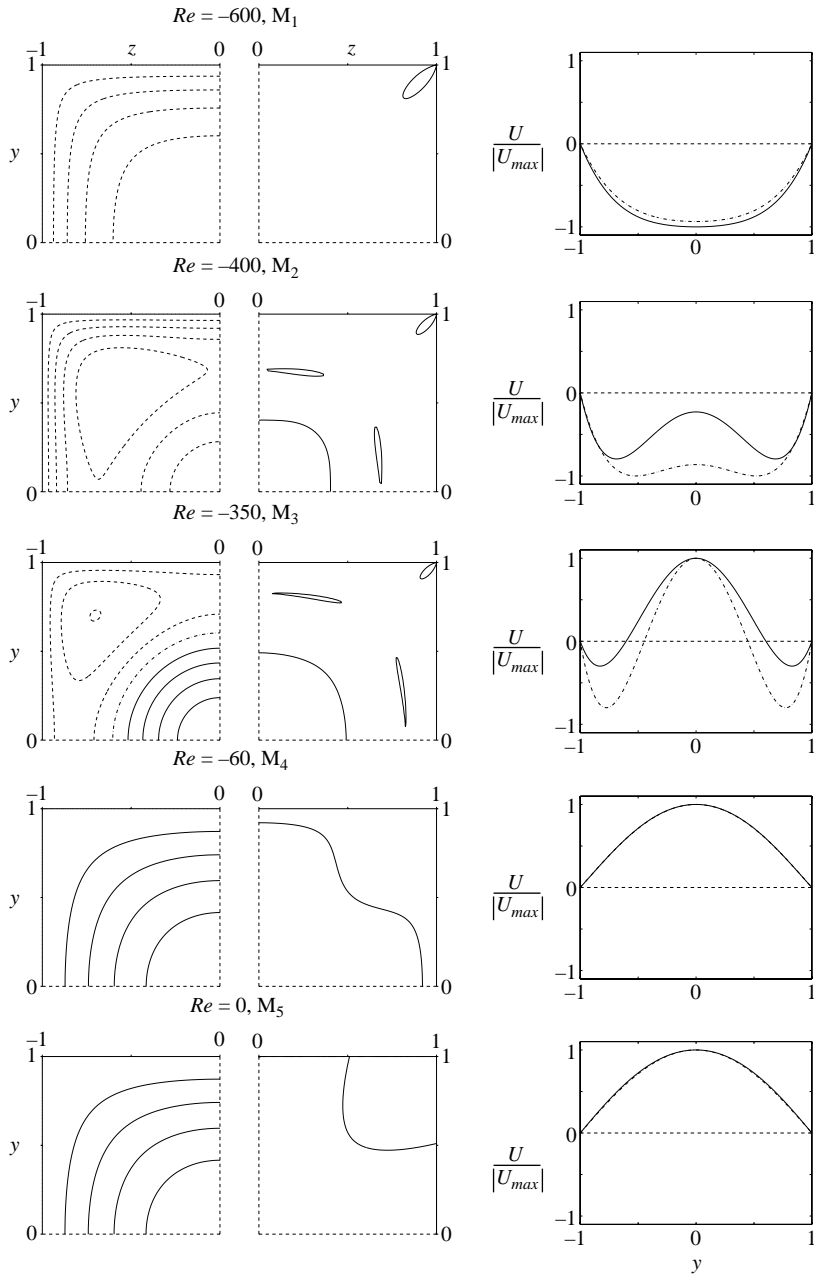


FIGURE 2. The basic flow of the square duct ( $A = 1$ ) with  $Gr = 3000$  and varying the Reynolds number such as to fall into the five ranges depicted in figure 1: isocontours of the basic flow velocity (graphs in first column) at values  $U/|U_{max}| = -1(0.2)1$  with negative values drawn by dashed lines; isocontours of  $d^2U/dn^2 = 0$  (graphs in second column). These basic flow types are distinguished by the difference in the number of disjoint inflection lines, except for type  $M_3$  which corresponds to the occurrence of reverse flow. Note that the basic flow is doubly symmetric and, therefore, only one quadrant is shown. The graphs in the third column show velocity profiles on the centreline,  $U(y, z=0)$ : —, square duct; - · -,  $A = \infty$ . In the case with  $A = \infty$ , the values for the Reynolds number are  $Re = -1670, -1375, -1200, -60, 0$  (from top to bottom).

---

$A$	$s_1$	$s_2$	$s_3$	$s_4$
1		-5.75	-7.69	-48.40
3	-1.07	-2.12	-2.55	-21.68
5	-0.62	-2.01	-2.41	-20.62
$\infty$		-2	-2.4	-3

---

TABLE 3. Slopes of the lines dividing the regions of the basic flow in the  $(Re, Gr)$ -plane, defined by  $Gr = s_i Re$  (cf. figure 1) for various aspect ratios  $A$ . The values have been obtained by evaluating inflectional properties of numerically obtained basic flow, except for the limit  $A = \infty$  which corresponds to the analytical profile of Nagata & Generalis (2002). Note that the region  $M_0$  and, therefore, the line with slope  $s_1$  only exists for intermediate aspect ratios.

---

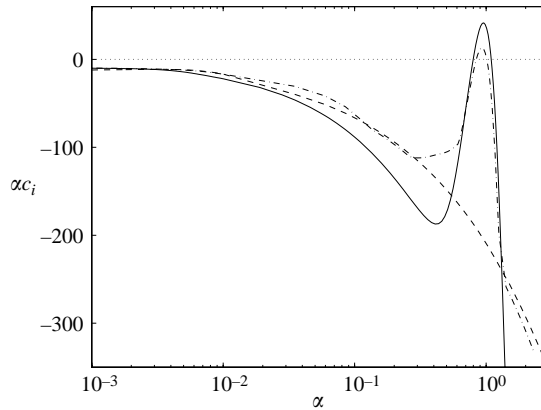


FIGURE 3. Growth rate *vs.* streamwise wavenumber for linear stability of the isothermal rectangular duct at  $Re = 10\,000$  and various aspect ratios: ---,  $A = 1$ ; - · -,  $A = 6$ ; —,  $A = \infty$ . These results were computed with truncation levels up to  $N_y = 30$ ,  $N_z = 60$ .

axis are the significant ones for the stability of the flow. When adopting the above definition of region  $M_2$  we find that the slopes of all dividing lines between basic flow regions decrease monotonously with the aspect ratio (cf. table 3). In the following, the usefulness of the proposed regions will become clear when strong correlations with the appearance of unstable modes are observed (cf. §4.2).

#### 4.2. Linear stability

In the isothermal case ( $Gr = 0$ ), the square duct ( $A = 1$ ) is now believed to be linearly stable (Tatsumi & Yoshimura 1990; Theofilis *et al.* 2004). Above a critical aspect ratio ( $A_{c,iso} = 3.2$ ) a modulated analogue of the wall-mode which is responsible for instability in PPF becomes unstable. Figure 3 illustrates the situation for  $Re = 10\,000$  and  $A = 1, 6, \infty$ . For  $A = 1$ , the maximum growth rate is found at small wavenumbers ( $\alpha \approx 0.005$ ). However, this feature disappears with increasing aspect ratio and only the above mentioned wall-mode eventually becomes unstable (cf. analogue discussion for elliptic pipe flow by Kerswell & Davey 1996).

The effect of internal heating upon pressure-driven flow in a plane channel can be conveniently demonstrated in the  $(Re, Gr)$ -plane. For this purpose, we have re-computed the linear results of Nagata & Generalis (2002) for vanishing Prandtl number and obtained additional data at  $Pr = 7$  (finite Prandtl numbers were previously considered in Generalis & Nagata 2003, but only for vanishing Reynolds



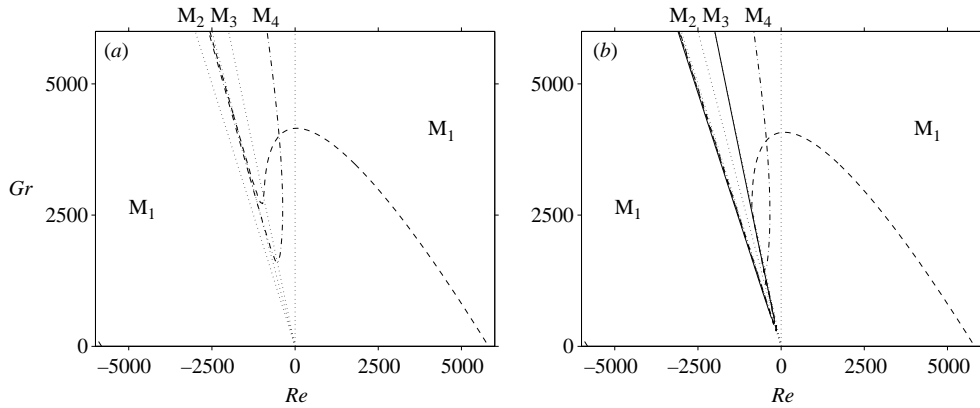


FIGURE 4. Neutral curves for heated and pressure-driven plane flow ( $A = \infty$ ) at (a)  $Pr = 0$  and (b)  $Pr = 7$ , and various values for the streamwise wavenumber: —,  $\alpha = 0.5$ ; ---,  $\alpha = 1$ ; — · —,  $\alpha = 1.5$ . The straight dotted lines indicate the boundaries of the basic flow regions ( $M_1$  to  $M_5$ ) for this specific configuration. In all cases, the mode with antisymmetric parity of the streamwise velocity (i.e.  $u(o, \cdot)$ , where  $\cdot$  indicates that there is no variation in  $z$ ) is the most unstable.

numbers). Figure 4 shows the neutral curves at various values for the streamwise wavenumber for  $A = \infty$ . It can be seen that for a range of wavenumbers, the flow loses stability in a conical area coinciding mostly with basic flow region  $M_3$  (where additional inflection lines and reverse flow are found); for finite Prandtl numbers, the conical area also includes parts of region  $M_2$ . With increasing Prandtl number, these cones tend towards the  $Gr = 0$  axis. For wavenumbers around  $\alpha = 1$ , the unstable area broadens towards the first quadrant and connects to the purely hydrodynamic mode which is found on the axis  $Gr = 0$  at  $|Re| = 5772.22$  (Orszag 1971). In the second quadrant of the  $(Re, Gr)$ -plane Orszag's mode is connected to an unstable region extending towards higher negative Reynolds numbers.

Turning to the configuration with finite aspect ratio, the first question is whether the heated square duct ( $A = 1$ ) allows for linearly unstable modes in the limit of vanishing Prandtl number. We recall that this limit corresponds to Tatsumi & Yoshimura's analysis, albeit for a modified basic flow. For this purpose, we have swept the parameter space in the following range:

$$Pr = 0, \quad Re \in [-50\,000, 50\,000], \quad Gr \in [0, 8000], \quad \alpha \in [0.1, 3],$$

for all three different symmetry modes (I=IV, II and III) and using truncation levels up to  $N_y = N_z = 35$ . No unstable modes could be detected. Figure 5(a) shows corresponding curves of the growth rate as a function of the streamwise wavenumber at a fixed value for the Grashof number ( $Gr = 3000$ ); the values for the Reynolds number are chosen such as to represent all basic flow types of figures 1 and 2. By comparison with figure 3, it can be observed that the homogeneous heat release has a general destabilizing effect upon the flow and that the effect is strongest when the pressure-gradient and the buoyancy are opposed (i.e.  $GrRe < 0$ ). In particular, the growth rate is largest when the basic flow has additional inflection lines (region  $M_2$ ), with a broad peak around  $\alpha = 1$ .

Setting the Prandtl number to a finite value causes an additional destabilization of the flow. From figure 5(b), where growth rates for  $Pr = 7$  are shown, it becomes clear

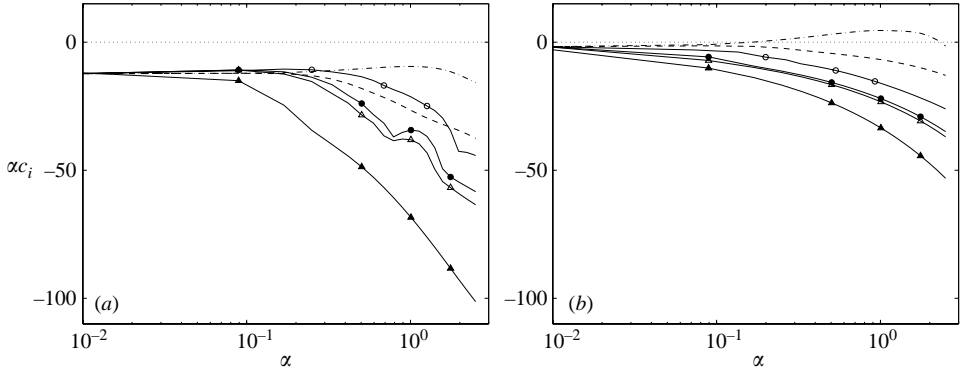


FIGURE 5. Growth rate *vs.* streamwise wavenumber for linear stability of the heated square duct ( $A=1$ ,  $Gr=3000$ ) at vanishing and finite Prandtl number and various values for the Reynolds number: ---,  $Re=-600$  (basic flow region  $M_1$ ); -·-,  $Re=-400$  ( $M_2$ ); -○-,  $Re=-200$  ( $M_3$ ); —●—,  $Re=-60$  ( $M_4$ ); —△—,  $Re=0$  ( $M_5$ ); —▲—,  $Re=600$  ( $M_1$ ). (a)  $Pr=0$ , (b)  $Pr=7$ . The symmetry corresponds to mode I, which is always the most unstable. The truncation level is  $N_y=N_z=20$ .

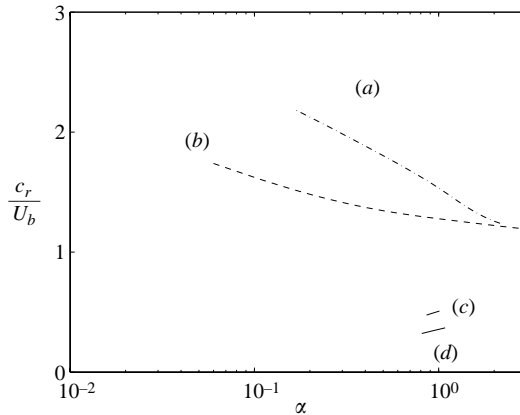


FIGURE 6. Phase velocity *vs.* streamwise wavenumber for the unstable modes in purely pressure-driven and heated duct flow: (a) square duct in region  $M_2$  ( $A=1$ ,  $Gr=3000$ ,  $Pr=7$ ,  $Re=-400$ , cf. figure 5); (b) heated PPF in region  $M_2$  ( $A=\infty$ ,  $Gr=3000$ ,  $Pr=7$ ,  $Re=-1375$ ); (c) isothermal duct with  $A=6$ ,  $Re=10\,000$  (cf. figure 3); (d) isothermal PPF with  $Re=10\,000$  (cf. figure 3).

that the growth rate is enhanced for all  $(Gr, Re)$ -pairs with respect to the  $Pr=0$  case; instability is obtained for the curve representing region  $M_2$  and symmetry mode I.

These new unstable modes can be distinguished from the ‘wall modes’ found in the isothermal case (at much higher Reynolds number and at larger aspect ratio) by considering the phase velocity  $c_r$ . In order to account for variations of the basic flow from case to case, the ordinate in figure 6 has been normalized by the bulk velocity,

$$U_b = \int_{-A}^A \int_{-1}^1 U(y, z) dy dz / 4A.$$

It can be seen that for the unstable perturbations of figure 5(b), the phase velocity varies between  $1.2U_b$  and  $2.2U_b$ , similar in magnitude to the corresponding case of

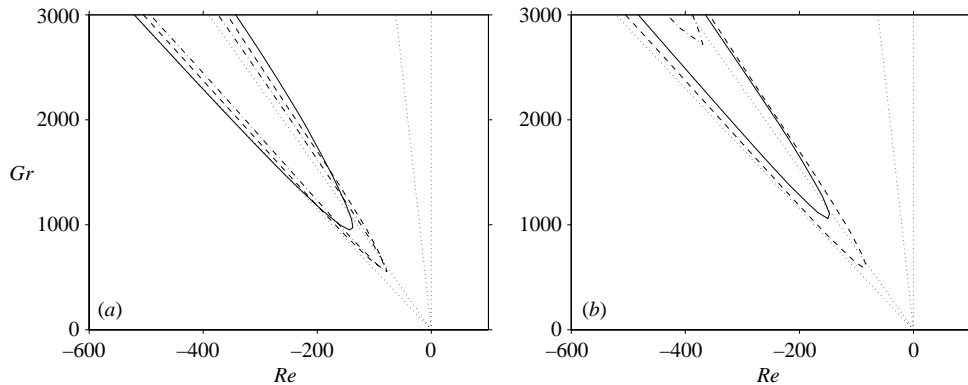


FIGURE 7. Neutral curves for heated and pressure-driven square duct flow ( $A=1$ ). (a) Finite Prandtl number ( $Pr=7$ ) and various values for the streamwise wavenumber: —,  $\alpha=0.5$ ; ---,  $\alpha=1$ ; - · -,  $\alpha=1.5$ ; (b) Streamwise wavenumber  $\alpha=1$  and various values for the Prandtl number: - · -,  $Pr=1$ ; —,  $Pr=3$ ; ---,  $Pr=7$ . The straight dotted lines indicate the boundaries of the basic flow regions (cf. figure 1). The symmetry mode I is always the most unstable. The truncation level is  $N_y=N_z=20$ .

HPPF. As a comparison, Tatsumi's and Orszag's modes propagate at a much slower velocity of  $0.3U_b, \dots, 0.6U_b$ . The high values for the phase velocity of the unstable modes in the heated case mean that critical lines – if they exist – are located near the maxima of the basic flow found in the central region of the channel. Furthermore, figure 6 shows a broad excitation of streamwise wavenumbers for the present case of internally heated flow, as opposed to the localized peaks of the isothermal case.

The relation between the inflectional properties and the instability of flow in the heated duct becomes clear when considering the neutral curves in the  $(Gr, Re)$ -plane (figure 7). For  $Pr=7$  and  $\alpha=0.5, 1, 1.5$  the instability is confined to a conical area coinciding roughly with the basic flow region  $M_2$ . As opposed to the HPPF case (cf. figure 4), the dependency upon the value of the streamwise wavenumber is small and zones  $M_1, M_4, M_5$  and most of zone  $M_3$  are stable. When increasing the value of the Prandtl number between  $Pr=1$  and  $Pr=7$  the extent of the conical region of instability grows towards the origin of the diagram (figure 4b). The striking match between the proposed partitioning of the  $(Gr, Re)$ -plane by means of the inflection property and the linear instability underline the importance of the inflectional nature of the basic flow for the heated duct.

The eigenvalue spectrum is modified owing to internal heat release, as can be seen from figure 8. In this figure, the isothermal situation is compared to the case with finite Grashof number, for vanishing and finite values of the Prandtl number, while the Reynolds number is kept at a constant value of  $Re=-400$ . Since the basic flow varies between the former and the latter two cases, we again normalize the real part of the complex phase velocity with the bulk velocity  $U_b$ . By varying the resolution up to  $N_y=N_z=40$  it has been verified that these eigenvalues have converged to within  $10^{-4}$  in the units of figure 8. In the isothermal case, multiple branches with  $c_i \rightarrow -\infty$  are found in the range  $0.4 \leq c_r/U_b \leq 1.4$ . Note that in the limit  $A=\infty$  only a single such branch with  $c_r=U_b$  exists. (Theofilis *et al.* (2004) present the eigenvalue spectrum for  $A=1$  and  $Re=100$  in the isothermal case (their figure 4), however, without specifying the value for the streamwise wavenumber. It was checked that the wavenumber was in fact set to  $\alpha=0.5$  in their computation (V. Theofilis,

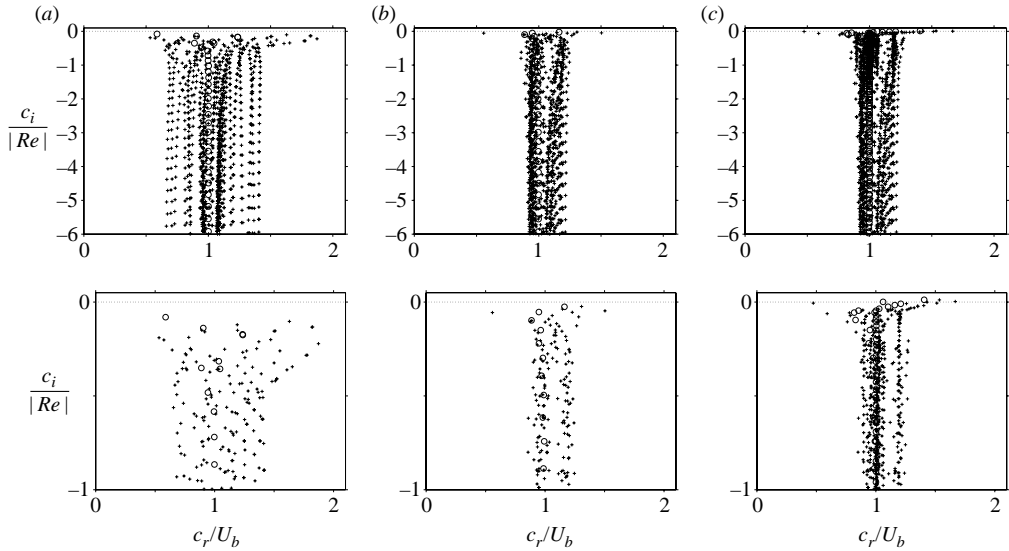


FIGURE 8. Eigenvalue spectra for  $Re = -400$  and  $\alpha = 1$  in the square duct case,  $A = 1$ , with (a)  $Gr = 0$ ,  $Pr = 0$  (isothermal); (b)  $Gr = 3000$ ,  $Pr = 0$  (heated, but no temperature fluctuations); (c)  $Gr = 3000$ ,  $Pr = 7$ . Note that only the case (c) has eigenvalues with positive growth rate. The open circles correspond to the limit  $A = \infty$  at the same Reynolds and Prandtl number values with (a)  $Gr = 0$ ; (b)  $Gr = 880$ ; (c)  $Gr = 880$ . The graphs on the bottom show the same data in a close-up view of the most unstable modes. Convergence of the eigenvalues to within  $10^{-4}$  (complex norm, in the units of the graphs) was confirmed by varying the resolution up to  $N_y = N_z = 40$ .

personal communication). It was also verified that for matching wavenumbers, we obtain a perfect agreement with the data of Theofilis *et al.* (2004).) In the heated cases ( $Gr = 3000$ ), these branches are visibly more concentrated around  $c_r = U_b$ . The main effect of the temperature fluctuations (i.e. finite Prandtl number, figure 8c vs. 8b) seems to be a shift of eigenvalues towards larger growth rates without changing the overall shape of the spectrum.

The three most unstable eigenfunctions for the heated and finite-Prandtl-number case (at the parameter point of figure 8c) are shown in figures 9–11. These belong to symmetry modes I, II and III, the first two being unstable and the latter one having a slightly negative growth rate. The graphs show contours of the streamwise velocity perturbation in the cross-stream plane as well as isosurfaces of the intensity  $|\mathbf{u}|$  of the perturbation velocity over one streamwise period and at arbitrary phase. All three eigenmodes exhibit smooth spatial structures. The highest intensities are located roughly halfway between the centre of the duct and the walls, in the direct vicinity of the inflection curves found in the core region of the duct.

We now turn our attention to geometries with finite aspect ratios above unity. For this purpose we will consider the values  $A = 3, 5$  – the former smaller than  $A_{c,iso}$  and the latter larger than  $A_{c,iso}$ . The corresponding curves in the heated case for  $Pr = 7$  and various streamwise wavenumbers are shown in figures 12–13. In both cases, the unstable region coincides mostly with basic flow region  $M_2$ , exhibiting incursions into the neighbouring region  $M_3$  for some values of the wavenumber. It should be emphasised that no unstable modes were found in zone  $M_0$  where all inflection curves are located away from the minor axis. This observation confirms that it is important

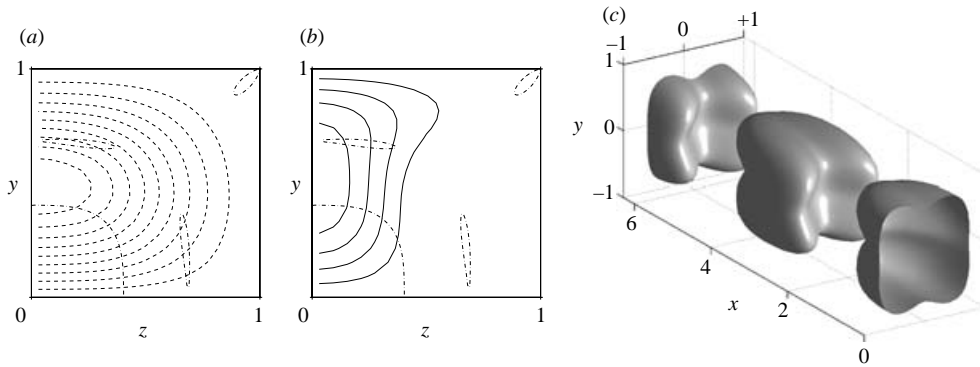


FIGURE 9. The most unstable eigenfunction in the square duct ( $A = 1$ ) at  $Gr = 3000$ ,  $Re = -400$  (zone  $M_2$ ,  $-43.825 \leq U \leq 0$ ),  $\alpha = 1$  and  $Pr = 7$  with  $c = -42.0095 + 4.5720i$ . (a) Real part of the streamwise velocity; (b) imaginary part; (c) isosurface of the intensity of the velocity perturbation  $|u|/\max|u| = 0.5$ , shown over one period and at arbitrary phase. In (a) and (b) the eigenfunction has been normalized such that  $\text{Im}(u(y = 0.5, z = 0.5)) = 0$  and  $\max(|\text{Re}(u)|) = 1$ . Contour lines are shown at intervals of 0.1 with negative values dashed. The chain-dotted lines indicate the inflection curves. This perturbation has symmetry mode I and only the first quadrant is shown in (a), (b). The truncation level is  $N_y = N_z = 25$ .

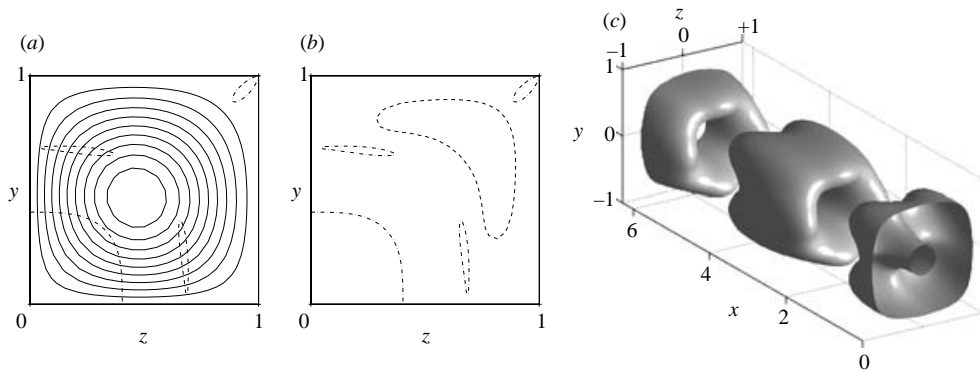


FIGURE 10. As figure 9, but showing the second most unstable mode with symmetry II. The corresponding eigenvalue is  $c = -45.6559 + 1.1916i$ .

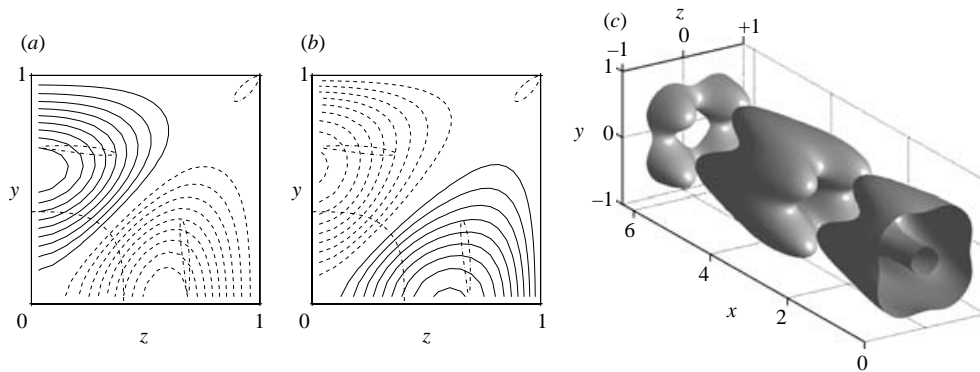


FIGURE 11. As figure 9, but showing the third most unstable mode with symmetry III. The corresponding eigenvalue is  $c = -39.1638 - 0.2725i$ .

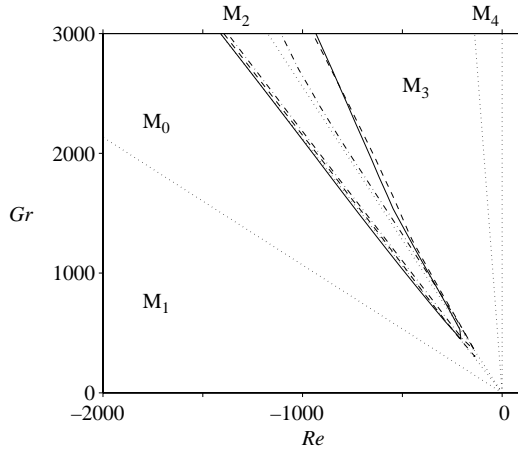


FIGURE 12. Neutral curves for heated and pressure-driven duct flow with aspect ratio  $A = 3$  at  $Pr = 7$  and various values for the streamwise wavenumber: —,  $\alpha = 0.5$ ; ---,  $\alpha = 1$ ; - · -,  $\alpha = 1.5$ . The straight dotted lines indicate the boundaries of the basic flow regions. The symmetry mode I is always the most unstable. The truncation level is  $N_y = 20$ ,  $N_z = 25$ .

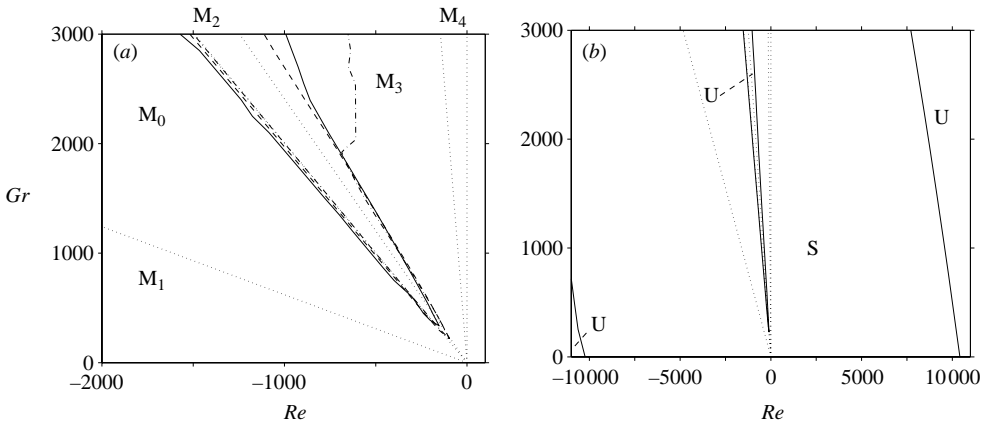


FIGURE 13. Neutral curves for heated and pressure-driven duct flow with aspect ratio  $A = 5$  at  $Pr = 7$  and various values for the streamwise wavenumber: (a) —,  $\alpha = 0.5$ ; ---,  $\alpha = 1$ ; - · -,  $\alpha = 1.5$ ; (b) —,  $\alpha = 0.91$ . In (b), the stable and unstable regions are marked by 'S' and 'U', respectively, for clarity. The straight dotted lines indicate the boundaries of the basic flow regions. The symmetry mode I is always the most unstable. Note that the ranges of the abscissae are different in the two graphs. The truncation level is  $N_y = 20$ ,  $N_z = 25, \dots, 35$ .

to distinguish between the basic flow regions  $M_0$  and  $M_2$  in the rectangular geometry. The comparison of figures 7, 12 and 13 shows that the main effect of increasing the aspect ratio in this moderate range is a growth of the conical region of instability towards the origin of the  $(Re, Gr)$ -plane. Figure 13(b) shows the neutral curves for the duct with  $A = 5$  and a wavenumber of  $\alpha = 0.91$ , the value identified by Tatsumi & Yoshimura (1990) as critical (for  $|Re| \geq 10\,400$ ) in the isothermal case. It can be seen that – within the present range of values for the Grashof and Reynolds numbers – the ‘thermal modes’, i.e. those in the conical region overlapping with  $M_2$ , do not

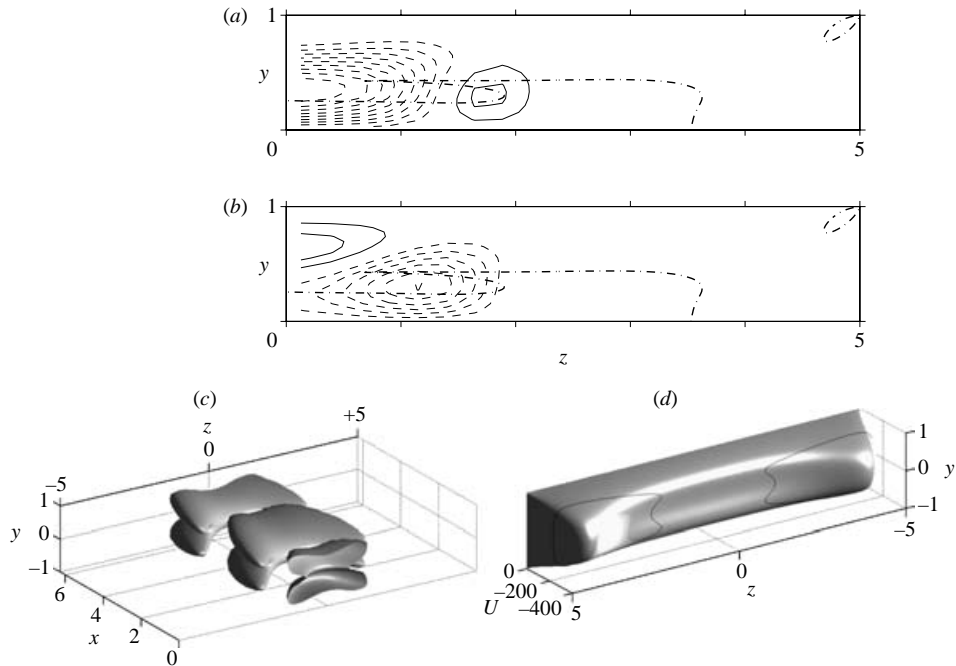


FIGURE 14. The most unstable eigenfunction of the duct with aspect ratio  $A = 5$  at  $Gr = 3000$ ,  $Re = -1400$  (zone  $M_2$ ,  $-322.039 \leq U \leq 0$ ),  $\alpha = 1$  and  $Pr = 7$  with  $c = -172.2463 + 5.9927i$ . This perturbation has symmetry mode I. Otherwise, notation and normalization as in figure 9. The additional graph (d) shows a surface plot of the basic flow velocity with the critical line  $U = c_r$  marked in black. The truncation level is  $N_y = 25$ ,  $N_z = 30$ .

reconnect with Tatsumi's modes located on the  $Gr = 0$  axis. In particular, the neutral curve emerging from the  $Gr = 0$  axis at  $Re = +10\,400$  follows an almost straight line which is slightly tilted towards the  $Re = 0$  axis. We have not checked whether both unstable zones might connect for even larger values of the Grashof number (as in the HPPF case, cf. figure 4b).

Finally, the eigenfunction of the most unstable perturbation in the rectangular duct with aspect ratio  $A = 5$  and choosing a parameter point in zone  $M_2$  ( $Gr = 3000$ ,  $Re = -1400$ ,  $Pr = 7$ ,  $\alpha = 1$ ) is depicted in figure 14. This eigenmode has a positive growth rate and belongs to symmetry mode I. The highest intensities of the perturbation are concentrated near the centre of the duct, being approximately confined to  $|z| \leq 2$ . Their location again correlates strongly with the position of the central inflection curve. The plots in figure 14 underline the fact that the present perturbations are distinct from the unstable modes found by Tatsumi & Yoshimura (1990), which, by contrast, exhibit a strong shear layer in the corner region (cf. their figure 5) and a low phase velocity.

Figure 15 shows a cut of this eigenfunction along the minor axis and compares it to the case of the plane channel geometry at a corresponding parameter point in the basic flow zone  $M_2$  ( $Gr = 880$ ,  $Re = -400$ ,  $\alpha = 1$ ; the most unstable mode of the spectrum shown in figure 8c). The similarities are found to be very strong, indicating that the perturbations at intermediate aspect ratios can be considered as 'spanwise-modulated variants of the plane eigenmodes'.

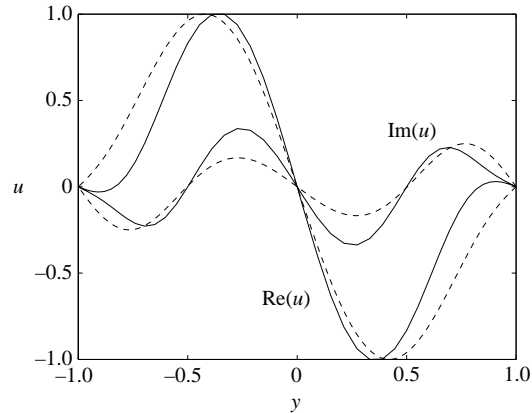


FIGURE 15. Comparison of the most unstable perturbation for the channel with  $A=5$  of figure 14 on the axis  $z=0$  (solid line) with the corresponding perturbation in the plane channel, at the parameter point of figure 8 (c) (dashed line). The eigenfunctions are normalized such that  $\text{Im}(u(y=0.5))=0$  and  $\max(|\text{Re}(u)|)=1$ .

## 5. Conclusion

The linear stability of fully developed laminar flow in a vertically oriented rectangular duct, being subject to homogeneous internal heating and an external pressure gradient, has been investigated numerically. We have proposed a classification of the basic flow with respect to inflection properties and the occurrence of reverse flow, leading to the definition of six distinct types of velocity profile which are uniquely defined by the ratio between the Grashof number and the Reynolds number. Values for the slopes of the lines separating the regions in the  $(Re, Gr)$ -plane where these basic flow types occur have been determined at selected aspect ratios, showing a monotone tendency towards the analytical values in the limit of a plane channel (Nagata & Generalis 2002).

Our stability analysis has revealed a new class of unstable modes for duct flow. In the square geometry, perturbations with positive growth rates only exist for finite values of the Prandtl number which implies that the equation for the temperature fluctuations must be included in the analysis. These new instabilities encompass all possible symmetry modes, with mode I (in the terminology of Tatsumi & Yoshimura 1990) found to be the most unstable. The unstable region in the  $(Re, Gr)$ -plane is roughly wedge-shaped and corresponds to basic flow profiles exhibiting additional inflection lines which cross the minor axis, i.e. the neutral curves are contained in basic flow zones  $M_2$  and  $M_3$  in our notation. Furthermore, these perturbations were found to have a positive growth rate over a broad range of streamwise wavenumbers. They have the noteworthy property of a high phase velocity, comparable in size to the maximum basic flow velocity. The corresponding eigenfunctions exhibit a large-scale bulge-like shape with their highest intensities located near the inflectional lines in the centre of the cross-section. The new class of perturbations is, therefore, of a distinct nature from the ‘wall modes’ which were found by Tatsumi & Yoshimura (1990) in the isothermal case and which become unstable only at high Reynolds numbers and for large aspect ratios. Finally, it was shown that, across the minor axis, the current modes at intermediate values of the aspect ratio bear a strong resemblance to their counterparts in the plane geometry.



Our results open the door for a subsequent nonlinear analysis. At first, the secondary flow solutions bifurcating from the present perturbations should be explored. The following step will then be an attempt at finding nonlinear solutions for the isothermal case by means of a continuation technique (homotopy). This requires tracking the secondary flow down to the limit of vanishing Grashof number. Obviously, there is no guarantee of the success of this approach as the solution branch might lead away from the desired limit (as e.g. in pipe flow with added system rotation, Barnes & Kerswell 2000). Currently, work on these aspects of the nonlinear stability of duct flow is underway.

M.U. was supported by the Spanish Ministry of Education and Science under contract DPI-2002-040550-C07-04 and acknowledges a grant from the Japanese Society for the Promotion of Science (Postdoctoral Fellowship for Foreign Researchers, P03753).

## REFERENCES

- BARNES, D. & KERSWELL, R. 2000 New results in rotating Hagen–Poiseuille flow. *J. Fluid Mech.* **417**, 103–126.
- EHRENSTEIN, U. & KOCH, W. 1991 Three-dimensional wavelike equilibrium states in plane Poiseuille flow. *J. Fluid Mech.* **228**, 111–148.
- GALLETTI, B. & BOTTARO, A. 2004 Large-scale secondary structures in duct flow. *J. Fluid Mech.* **512**, 85–94.
- GAVRILAKIS, S. 1992 Numerical simulation of low-Reynolds-number turbulent flow through a straight square duct. *J. Fluid Mech.* **244**, 101–129.
- GENERALIS, S. & NAGATA, M. 2003 Transition in homogeneously heated inclined plane parallel shear flows. *J. Heat Transfer* **125**, 795–803.
- GILCHRIST, J., KRIEGSMANN, G. & PAPAGEORGIOU, D. 1998 Stability of a microwave heated fluid layer. *IMA J. Appl. Maths* **60**, 73–89.
- KAO, T. & PARK, C. 1970 Experimental investigations of the stability of channel flows. Part 1. Flow of a single liquid in a rectangular channel. *J. Fluid Mech.* **43**, 145–164.
- KAWAHARA, G., JIMÉNEZ, J., UHLMANN, M. & PINELLI, A. 1998 The instability of streaks in near-wall turbulence. *CTR Annu. Res. Briefs, Stanford University*, pp. 155–170.
- KERSWELL, R. & DAVEY, A. 1996 On the linear instability of elliptic pipe flow. *J. Fluid Mech.* **316**, 307–324.
- KIKUCHI, Y., SHIOYAMA, T. & KAWARA, Z. 1986 Turbulent heat transport in a horizontal fluid layer heated internally and from below. *Intl J. Heat Mass Transfer* **29**, 451–461.
- McKENZIE, D., ROBERTS, J. & WEISS, N. 1974 Convection in the Earth's mantle: toward a numerical simulation. *J. Fluid Mech.* **62**, 465–538.
- NAGATA, M. 1990 Three-dimensional finite-amplitude solutions in plane Couette flow: bifurcation from infinity. *J. Fluid Mech.* **217**, 519–527.
- NAGATA, M. & GENERALIS, S. 2002 Transition in convective flows heated internally. *J. Heat Transfer* **124**, 635–642.
- NOURGALIEV, R. & DINH, T. 1997 The investigation of turbulence characteristics in an internally-heated unstably-stratified fluid layer. *Nucl. Engng Design* **178**, 235–258.
- ORSZAG, S. 1971 Accurate solution of the Orr–Sommerfeld equation. *J. Fluid Mech.* **50**, 689–703.
- ROBERTS, P. 1967 Convection in horizontal layers with internal heat generation: theory. *J. Fluid Mech.* **30**, 33–49.
- SHEN, J. 1995 Efficient spectral-Galerkin method II. Direct solvers of second and fourth order equations by using Chebyshev polynomials. *SIAM J. Sci. Comput.* **16**, 74–87.
- TATSUMI, T. & YOSHIMURA, T. 1990 Stability of the laminar flow in a rectangular duct. *J. Fluid Mech.* **212**, 437–449.
- THEOFILIS, V., DUCK, P. & OWEN, J. 2004 Viscous linear stability analysis of rectangular duct and cavity flows. *J. Fluid Mech.* **505**, 249–286.

- TRITTON, D. 1975 Internally heated convection in the atmosphere of Venus and in the laboratory. *Nature* **257**, 110–112.
- TRITTON, D. & ZARRAGA, M. 1967 Convection in horizontal layers with internal heat generation: experiments. *J. Fluid Mech.* **30**, 21–32.
- UHLMANN, M. 2004 Linear stability analysis of flow in an internally heated rectangular duct. *Tech. Rep.* 1043, CIEMAT, Madrid, Spain, ISSN 1135-9420.
- WALEFFE, F. 2001 Exact coherent structures in channel flow. *J. Fluid Mech.* **435**, 93–102.
- WEDIN, H. & KERSWELL, R. 2004 Exact coherent structures in pipe flow: travelling wave solutions. *J. Fluid Mech.* **508**, 333–371.